EJNMMI Physics

ORIGINAL RESEARCH Open Access

From SPECT/CT towards absolute quantification? - the case of unilateral condylar hyperplasia of the mandible

Stijn De Schepper[1,2*], Gopinath Gnanasegaran[3], Wouter De Vos[4,5], Elke Van de Casteele[4,5], John C. Dickson[6] and Tim Van den Wyngaert[1,2]

*Correspondence:
Stijn De Schepper
stijn.deschepper@uza.be
[1]Department of Nuclear Medicine, Antwerp University Hospital, Drie Eikenstraat 655, Edegem 2650, Belgium
[2]Faculty of Medicine and Health Sciences (MICA – IPPON), University of Antwerp, Wilrijk, Belgium
[3]Department of Nuclear Medicine, Royal Free London NHS, London, UK
[4]Department of Oral and Maxillofacial Surgery, Antwerp University Hospital, Antwerp, Belgium
[5]Faculty of Medicine and Health Sciences, University of Antwerp, Wilrijk, Belgium
[6]Institute of Nuclear Medicine, University College of London Hospitals NHS, London, UK

Abstract

Background Unilateral condylar hyperplasia (UCH) of the mandible is a rare condition characterized by asymmetric growth of the mandibular condyles. Bone scintigraphy with SPECT(/CT) is commonly used to diagnose UCH and guide treatment. Still, varying results have been reported using the traditional threshold of 55%:45% in relative tracer uptake. While absolute quantification of uptake on SPECT/CT could improve results, optimal correction and reconstruction settings are currently unknown.

Methods Three anthropomorphic phantoms representing UCH were developed from patient CT volumes and produced using 3D printing technology. Fillable spherical inserts of different sizes (Ø: 8–15 mm) were placed in the condylar positions representing symmetrical and asymmetrical distributions. Recovery coefficients were determined for SPECT/CT using various reconstruction corrections, including attenuation and scatter correction (ACSC), resolution modeling (RM), and partial volume correction (PVC) using phantom measurements. Uptake ratios between condyles and condyle to clivus were evaluated. Finally, the impact of these correction techniques on absolute activity and diagnostic accuracy was assessed in a retrospective patient cohort for the diagnostic threshold of 55%:45%.

Results The activity was only partially recovered in all spherical inserts (range: 22.5–64.9%). However, RM improved relative recovery by 20.2–62.3% compared to ACSC. In the symmetric phantoms, the 95% confidence interval (CI) of condyle ratios included the diagnostic threshold (57.6%:42.4%) for UCH when using ACSC potentially leading to false positives, but not for ACSCRM datasets. Partial volume corrections coefficients from the NEMA IQ phantom was positionally dependent, with improvements seen performing PVC using coefficients derived from anthropomorphic phantoms. Retrospective application in a patient cohort showed only a weak linear correlation (R^2: 0.25–0.67) and large limits of agreement (9.6–12.5%) between different reconstructions. Up to 44% of patients were reclassified using the 55%:45% threshold. Using clinical outcome data, ACSCRM had highest sensitivity (91%; 95% CI 59–100%) and specificity (66%; 95% CI 47–81%), significantly improving specificity ($P=0.038$).

Conclusions Anthropomorphic phantoms were shown to be essential in determining optimal settings for acquisition, reconstruction, and analysis. SPECT/CT reconstructions with attenuation and scatter correction and resolution modeling are recommended and could improve specificity when using the 55%:45% threshold to assess condylar growth.

Keywords Quantitative SPECT/CT, Phantom, 3D printing, Recovery coefficient, Mandible, Unilateral condylar hyperplasia

Introduction

Unilateral condylar hyperplasia (UCH) is a rare condition characterized by an asymmetric growth of the mandibular condyles, be it through an increased duration or rate of growth on the affected side [1]. In severe cases, the asymmetric growth can result in malocclusion, impairing mastication, and oral health-related quality of life [2]. The cause of UCH is currently unknown, and treatment is limited to corrective surgery.

Bone scintigraphy using technetium-99m-labeled phosphate analogs such as [^{99m}Tc]-HDP [3] is indicated to identify UCH, by relative quantification of condylar tracer uptake as a sign of asymmetric bone remodeling, and to determine the optimal surgical approach [4]. Both planar scintigraphy and single-photon emission tomography (SPECT) acquisitions have traditionally been used for this purpose, considering a relative activity difference between condyles larger than 10% as evidence of asymmetric growth [5]. In addition, comparing condylar uptake with that in the clivus of the skull has been used to determine the residual active condylar growth in adolescents.

With the advent of hybrid imaging, SPECT/CT has replaced standalone SPECT for many applications, including bone imaging, where the technique has been shown to improve diagnostic accuracy and may contribute to improved patient outcomes [6, 7]. Despite this technological progress, several studies using SPECT and SPECT/CT for the semiquantitative assessment of the mandibular condyles have shown a considerable variation in the diagnostic performance for UCH [4, 5, 8–10]. This variability may partly result from differences in image acquisition and reconstruction methods, even though a formal evaluation is currently lacking. Awaiting further validation, the 55%:45% threshold remains the established clinical reference [4].

SPECT/CT also offers the possibility of quantitative reconstructions, using correction techniques that compensate for known image degrading effects [11–13]. However, the quantification of the mandibular condyles remains challenging because of the high density of bone causing attenuation and scatter; their close proximity to the articular surface of the temporomandibular joint, and their small size increases the partial volume effect (PVE). In addition, attenuation correction (AC) and scatter correction (SC) methods used in image reconstruction will affect the tracer distribution between condyles and the clivus differently, as the latter is located deeper within the skull. Similarly, it is known that resolution modeling (RM) within the reconstruction, which attempts to decrease the PVE, can introduce artefacts in the activity distribution, depending on the method and application [14]. For these reasons, several guidelines on quantitative SPECT/CT for dosimetry purposes recommend against the quantification of small tumors, yet guidance in other applications, such as bone imaging, is currently lacking [15, 16].

With the recent developments in 3D printing technology, increasingly complex phantoms have been developed for different anatomic structures and pathologies,

representing a ground truth to study the accuracy of absolute quantification in SPECT/CT [17–20]. These anthropomorphic phantoms can now be developed and produced with relative ease and reasonable cost, and provide an attractive platform to study situations where in vivo activity tissue measurements are not feasible. Nevertheless, while phantoms representing parts of the skeleton have been produced, there are no prior reports on anthropomorphic phantoms recapitulating an actual primary bone disease state [21].

The present study aimed to establish the optimal reconstruction and corrections for absolute quantification of bone SPECT/CT to evaluate bone growth of the mandibular condyles. For this, anthropomorphic phantoms of the normal and pathological anatomy were developed to serve as ground truth for the quantitative accuracy of SPECT/CT for bone-tracer uptake in the mandibular condyles, specifically in the pathological context of UCH. Finally, a retrospective patient dataset was used to assess the impact on diagnostic classification between the current clinical standard assessment method and thresholds based on absolute quantification using optimal reconstruction and corrections.

Materials and methods

Phantom development

Three anthropomorphic phantoms were created representing examples of bone anatomy of a normal patient and two patients positive for UCH, based on data from clinical CT studies (Fig. 1). Bone structures were segmented in 3D Slicer (v4.11.20210226; www.slicer.org). A shell of 2 mm thickness was created for the phantom using Meshmixer (Autodesk Inc., San Francisco, CA, USA) and divided into four parts for printing. Spherical inserts of different diameters (8 mm, 10 mm, 13 mm, and 15 mm) were placed in the phantoms using Inventor (v2021; Autodesk Inc., San Francisco, CA, USA) in the positions of the mandibular condyles. The spherical inserts are fillable through small access tubes.

A resin 3D printer (Form 3, FormLabs, Somerville, MA, USA) was used to print the phantoms in parts before final assembly. The quoted resolution of the printer (25 μm) far exceeded the ability to visually detect differences between prints of the same phantom.

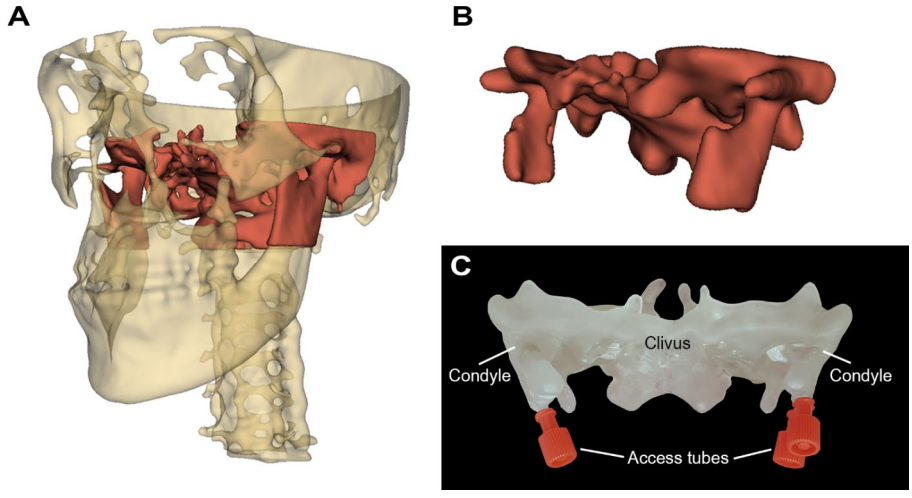

Fig. 1 (**A**) Segmentation of the bone structures of the skull. (**B**) Model of the corresponding anthropomorphic phantom. The red segmentation of the skull is the region representing the phantom. (**C**) Front view picture of the phantom with mounted access tubes for the condyle spheres and the background volume

The accuracy of the phantom was determined by the Dice coefficient, comparing the volumes of the phantoms with the bone segmentations on their respective patient CT studies [22]. A more detailed analysis of the printing accuracy exceeds the scope of the current study.

The anthropomorphic phantoms were filled with a clinically relevant spheres-to-background ratio of 3:1 with concentrations of [^{99m}Tc]-pertechnetate of 120 kBq/mL in the spheres and 40 kBq/mL in the background similar as determined from patient scans. The spheres on both sides were injected with the same activity concentration to test the smallest meaningful difference for symmetric size condyles and the PVE on the asymmetric phantoms. The background volume was filled with an HK_2O_4P-containing solution to mimic the attenuation of trabecular bone (1.05 g HK_2O_4P / g water) [23].

Patient cohort

Clinical datasets from consecutive patients referred to the nuclear medicine department of the Antwerp University Hospital from 2020 to 2022 to evaluate condylar growth were used if all pertinent data on administered activity and time were available. Patients were excluded if there was a history of craniofacial trauma or malignancy, or if the CT part of the study showed osteoarthritic changes in the temporomandibular joints. Clinical follow-up data was collected and used to determine the reference standard based on the composite of routine (post-operative) clinical follow-up. This study was approved by the ethics committee of the Antwerp University Hospital (N°: 5640).

SPECT/CT acquisition

All scans (patient and phantom) were performed on a GE Discovery 670 NM/CT 16 slice SPECT/CT camera with 3/8" NaI crystal (GE Healthcare, Haifa, Israel). LEHR collimators were used, and 120 projections were acquired. Each projection consisted of a 100-second (phantoms) or 25-second (patients) acquisition in a 128×128 matrix with 4.4×4.4 mm² pixels. Experiments were repeated using a matrix of 256×256 pixels, yielding identical findings (data not shown). Following the SPECT acquisition a CT image was acquired with tube voltage of 120 kV, tube current of 50 mA and slice thickness of 1.25 mm. The anthropomorphic phantoms were placed in a box to simulate clinical positioning and typical detector-to-patient distance in clinical scans.

The SPECT camera and radionuclide calibrator (VDC-405, Veenstra (Comecer), Castel Bolognese, Italy) are cross-calibrated using the planar sensitivity method according to the manufacturer's recommendations. Afterward, the absolute quantification was verified using a large cylindrical phantom of 6,283 mL. The camera sensitivity was measured and confirmed at 78.97 cps/MBq.

Image reconstruction and analysis

All image reconstructions were based on the ordered-subsets expectation and maximization (OSEM) algorithm as implemented in MIM (7.2.3, MIM Software Inc, Cleveland, OH, USA) and optimized prior to the start of the experiments (data not shown): 5 iterations and 20 subsets had the best activity recovery while limiting noise. Three reconstructions were made: "NAC" an OSEM reconstruction without corrections (in counts), "ACSC" an OSEM reconstruction including AC and SC, and "ACSCRM" an OSEM reconstruction including AC, SC, and RM. No post-reconstruction filter was applied.

The phantom measurements and patient data were reconstructed using identical settings. Image analyses of the phantom and patient data were subsequently performed in MIM. Numerical analyses were performed in MatLab (v2021a, The MathWorks Inc, Natick, MA, USA). Error estimation on the phantom data was done using the bootstrap method [24]. The phantom datasets were Poisson sampled for the error estimation using Xeleris IV (GE Healthcare, Haifa, Israel) to include 25% of the data so that the statistics would resemble the patient data. All cited error estimates represent a 95% confidence interval.

Given the small structures involved spill-over will be apparent and partial volume correction (PVC) is required to achieve quantitative accurate results. While several approaches have been proposed [25] and developed for PET/CT [26], only resolution modeling is currently commercially available. A commonly used method is the application of empirically determined recovery coefficients from a NEMA IQ phantom [11]. The NEMA phantom was filled with the same activities and activity ratio as the anthropomorphic phantom (120 kBq/mL:40 kBq/mL) and scanned for two different configurations of the spheres, which differed by turning the insert 180° for the second acquisition. The acquisition was lengthened to have similar statistics for the second acquisition.

The RCs applied in the PVC are the result of a fit using a two-parameter logistic function of the sphere volume v [27]:

$$RC\,(v) = 1 - \frac{1}{1 + \left(\frac{v}{a}\right)^b}. \tag{1}$$

The recovery curves from the NEMA phantom, and separately, using the asymmetric anthropomorphic phantoms were used for PVC. The PVC recovery curves were validated on the symmetric phantom for the ACSC and the ACSCRM reconstruction sets. All phantom experiments were repeated twice.

Phantom data

Only the quantitative reconstructions are considered for the phantom scans: "ACSC" and "ACSCRM". The tracer uptake was quantified using spherical volumes of interest (VOI). For the spherical inserts, the diameter of the VOI was the same as that of the insert. VOIs of 8 mm (symmetric phantom) and 10 mm (asymmetric phantoms) were selected for the clivus as they were the largest that could be included while allowing some distance to the phantom edges. Recovery Coefficients (RC) were obtained for each sphere by drawing a spherical VOI:

$$RC = \frac{A_{SPECT}}{A_{inj}} \tag{2}$$

where A_{SPECT} is the mean activity concentration measured in the VOI and A_{inj} the activity concentration injected based on the radionuclide calibrator.

The ratio of tracer uptake in the left sphere was defined as:

$$\frac{A_L}{A_L + A_R} \tag{3}$$

with A_L and A_R the activity concentration measured in the left and right condyles, respectively.

The ratio of tracer activity concentration of the condyle versus clivus was defined as:

$$\frac{A_{Condyle}}{A_{Condyle} + A_{Clivus}} \tag{4}$$

Patient data

All three reconstructions ("NAC", "ACSC", and "ACSCRM") were made for each scan to assess the potential impact on UCH classification of the applied reconstruction methods and the correction techniques. Although the NAC reconstruction is not quantitative, it may more closely reflect the SPECT only reconstructions previously reported in literature as information on reconstruction algorithm and settings were not always provided [4]. The clinical reference method of analysis consists of calculating the ratio of mean uptake in circular ROIs of the same size for both condyles on the NAC reconstruction. A scan is considered positive for UCH when the difference in uptake ratios between the pathological and the normal condyle exceeds 10% (55%:45%) [4]. Alternatively, thresholds of 12% and 8% are also considered [10]. Similarly, the mean condylar uptake was compared with the clivus using Eq. (4).

It is considered to represent residual condylar growth when the difference in ratios exceeds 10% [5]. Surgical intervention is typically postponed in the presence of either finding, and patients are followed longitudinally until normalization of uptake.

For PVC, the radius of the mandibular condyles was estimated using the measured anteroposterior and mid-lateral condylar lengths [28]. Although the mandibular condyles are not spherical, they can be approximated by an ellipsoid for which it has been demonstrated that the RCs are similar to those of a sphere with the same volume [20]. The radius of the equivalent sphere was defined using the measured lengths:

$$R = \sqrt[3]{abb}$$

where a and b are the length of the anteroposterior and mid-lateral lengths. The RCs from the anthropomorphic phantoms were applied for the equivalent spheres on both the ACSC and ACSCRM reconstructions. Identical contours were drawn on the ACSC and ACSCRM reconstructions. The Bland-Altman method was used to assess agreement in ratios between methods and the reference method [24].

The reclassification rate was calculated for the diagnosis of UCH using the different quantitative methods compared to the reference method (NAC). The McNemar test was used to assess significant differences compared to the reference method in the subsets of patients considered to be positive and negative for asymmetric or residual growth according to the clinical reference standard, respectively [29]. As no recovery coefficients were available for the clivus, only the asymmetric growth status using the 55%:45% threshold was considered in the PVC datasets.

Results

Phantoms

Bone segmentation resulted in a clean anatomical model that preserved several pivotal anatomical features, including the clivus, occipital condyle and the foramina for the internal carotid arteries. The fusion of both CT scans of the phantoms and the patients showed good visual agreement. A quantitative comparison through the Dice coefficient

[30] confirmed good agreement between the segmented bone structures on the patient CTs and their respective phantoms (symmetric phantom: 0.863; asymmetric phantom: 0.897). Both phantoms were filled with the same bone-equivalent solution, resulting in a mean density and standard deviation of 680±334 HU on CT and comparing favorably with the mean bone densities in the source CTs, with 791±456 HU and 637±460 HU for the symmetric and asymmetric datasets, respectively [31]. Spherical and background volumes of the phantoms are summarized in Table 1.

Activity recovery

The activity recovered in the spheres of the symmetric phantom for the ACSC reconstruction was 22.5% [19.1–25.7%] and 24.3 [22.7–26.5%] for the left and right sphere of 8 mm diameter, respectively, which increased to 30.8% [26.7–35.0%] and 29.2% [27.3–31.1%] in the ACSCRM reconstruction set (Table 2). The spheres of the asymmetric phantoms are considered according to their size. The activity recovery in the ACSC reconstruction was 30.6% [28.9–32.4%], 32.1% [30.9–33.1%], 38.5% [37.2–39.8%], and 42.6% [41.2–44.3%] for the spheres of 8 mm, 10 mm, 13 mm, and 15 mm, respectively. For the ACSCRM reconstruction, these values are increased to 39.8% [36.1–43.5%], 48.4% [46.2–50.4%], 62.5% [59.7–65.0%], and 64.9% [62.9–67.1%].

The activity recovered for the clivus region in the ACSC reconstruction was 63.1% [56.4–71.2%], 78.3% [71.8–83.9%], and 77.1% [72.6–81.8%] for the symmetric phantom, asymmetric phantom 1 and asymmetric phantom 2 respectively. When RM was applied, the recovery increased to 82.2% [73.9–91.5%], 103.4% [93.4-113.2%], and 94.8% [87.9-101.5%], respectively.

Ratios

The ratio for the condyles measured in the symmetric phantom was 47.9% [42.4–52.3%] for the ACSC reconstruction and 51.1% [47.0-54.9%] for ACSCRM. Although the true activity ratio was approached in both reconstructions, the 95% confidence interval of the ACSC reconstruction included values beyond the 55%:45% threshold, potentially leading to a false classification for active growth. The ratio for asymmetric phantom 1 (R>L) was 44.3% [42.4–46.2%] in the ACSC reconstruction set and 38.8% [35.9–41.7%] in the ACSCRM reconstruction set. The ratio for asymmetric phantom 2 (L>R) was 57.0% [56.0-58.2%] in the ACSC reconstruction set and 57.3% [56.2–58.7%] in the ACSCRM reconstruction set.

Partial volume correction

There was a large difference in the recovery curves of the spheres in the NEMA phantom depending on sphere position relative to the detector for the ACSC reconstruction set and ACSCRM reconstruction set (Fig. 2 and Supplementary Table 1). When extrapolating the recovery curves to an 8 mm sphere, a RC of 39.4% was found for configuration 1

Table 1 The three anthropomorphic phantoms developed for this work and their main properties

	Symmetric phantom	Asymmetric phantom 1	Asymmetric phantom 2
Patient CT	Normal	UCH positive	UCH positive
Volume	63 mL	78 mL	78 mL
Left sphere diameter	8 mm	8 mm	15 mm
Right sphere diameter	8 mm	13 mm	10 mm

Table 2 The results from the anthropomorphic phantom scans. The values between brackets correspond to the 95% CI

			Activity concentration [kBg/mL]			Recovery coefficient [%]		Ratios		
Recon corrections			True	AC SC	AC SC RM	AC SC	AC SC RM		AC SC	AC SC RM
Symmetric phantom	Left	Ø 8 mm	111.5	25.1 [21.3–28.6]	34.3 [29.8–39.1]	22.5 [19.1–25.7]	30.8 [26.7–35.0]	L/(R + L)	47.9 [42.4–52.3]	51.1 [47.0-54.9]
	Right	Ø 8 mm	111.5	27.1 [25.3–29.6]	32.6 [30.4–34.7]	24.3 [22.7–26.5]	29.2 [27.3–31.1]	L/(L + C)	52.5 [47.9–56.5]	53.8 [49.3–57.8]
	Clivus	Ø 8 mm	35.6	22.5 [20.1–25.4]	29.3 [26.-32.6]	63.1 [56.4–71.2]	82.2 [73.9–91.5]	R/(R + C)	54.7 [51.8–57.5]	52.8 [50.7–55.2]
Asymmetric phantom 1	Left	Ø 8 mm	117.3	36.0 [33.8–3.80]	46.6 [42.4–51.0]	30.6 [28.9–32.4]	39.8 [36.1–43.5]	L/(R + L)	44.3 [42.4–46.2]	38.8 [35.9–41.7]
	Right	Ø 13 mm	117.3	45.1 [43.7–46.7]	73.3 [70.0-76.2]	38.5 [37.2–39.8]	62.5 [59.7–65.0]	L/(L + C)	53.6 [51.0-56.1]	53.0 [49.3–56.3]
	Clivus	Ø 10 mm	40.0	31.3 [28.7–33.5]	41.3 [37.3–45.2]	78.3 [71.8–83.9]	103.4 [93.4-113.2]	R/(R + C)	59.3 [57.0-61.8]	64.0 [61.5–66.5]
Asymmetric phantom 2	Left	Ø 15 mm	105.3	44.8 [43.4–46.7]	68.3 [66.2–70.6]	42.6 [41.2–44.3]	64.9 [62.9–67.1]	L/(R + L)	57.0 [56.0-58.2]	57.3 [56.2–58.7]
	Right	Ø 10 mm	105.3	33.8 [32.6–34.8]	50.9 [48.6–53.1]	32.1 [30.9–33.1]	48.4 [46.2–50.4]	L/(L + C)	61.8 [60.3–63.3]	66.8 [65.4–68.1]
	Clivus	Ø 10 mm	35.9	27.7 [26.0-29.3]	34.0 [31.5–36.4]	77.1 [72.6–81.6]	94.8 [87.9-101.5]	R/(R + C)	55.0 [53.8–56.2]	60.0 [57.7–62.2]

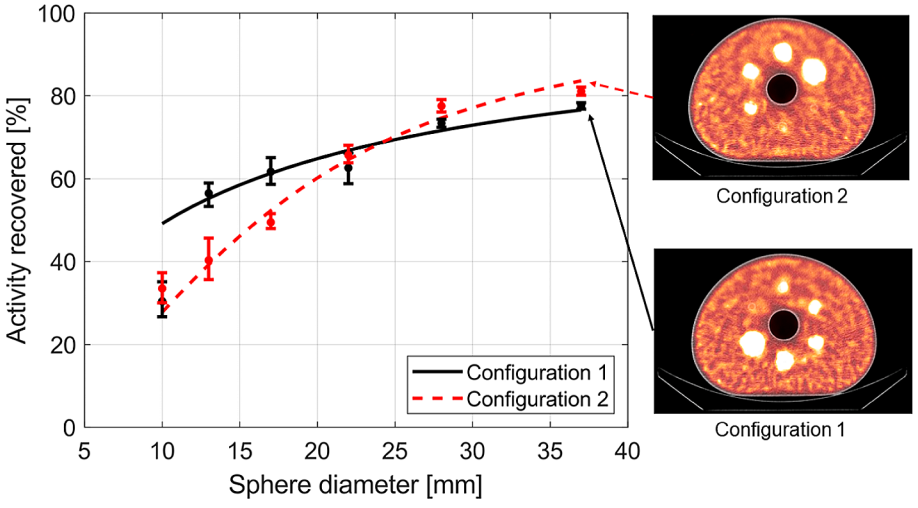

Fig. 2 The recovery curves of the 2 configurations of the NEMA IEC body phantom. The lines indicate the fitted curve with coefficients a = 581, b = 0.31 (Configuration 1) and a = 2233, b = 0.66 (Configuration 2)

and 23.5% for configuration 2 using the ACSC reconstruction set. When these RCs were applied to 8 mm spheres of the symmetric condyle phantom, this resulted in an overestimation of as much as 80% or an underestimation of up to 40% of the activity concentration, depending on the configuration choice. Alternatively, when PVC coefficients

were derived from the asymmetric phantoms, the activity recovered in the left and right spheres of the symmetric phantom increased to 74% [62–85%] and 80% [72-88%] without RM, and 78% [66–92%] and 75% [66–83%] with RM, respectively. There was no significant difference in the recovery of the spheres for the ACSC and ACSCRM reconstructions when their respective recovery curves were used (Fig. 3).

Patient cohort

Datasets from 27 patients were included, 11 female (41%) and 16 male (59%), totaling 43 bone SPECT/CT studies. One patient was excluded due to increased uptake as a result of trauma. No patients showed any signs of degenerative or inflammatory disease. There were 8 patients (30%) with a deviation of the jaw to the right, 15 patients (56%) with a deviation to the left, and 4 patients (15%) with suspected bilateral residual condylar growth. Patients were injected with a mean activity of 659±116 (SD) MBq of [^{99m}Tc]-HDP and scanned after 2.79±0.35 (SD) h. The affected condyles had a mean antero-posterior and mid-lateral length of 18.0±2.4 (SD) mm and 6.6±1.1 (SD) mm, while the contralateral condyles were, on average, smaller at 17.4±3.2 (SD) mm and 6.8±1.3 (SD) mm.

The comparisons of the ratios obtained using the ACSC and ACSCRM methods to the reference method are shown in Fig. 4. There was a very weak correlation between all methods, with correlation coefficients of $R^2 = 0.25$ for the NAC and ACSC sets, $R^2 = 0.40$ for the NAC and ACSCRM sets, and $R^2 = 0.32$ for the ACSC and ACSCRM sets. Similarly, the Bland-Altman plots show poor agreement between the different methods, with limits of agreement ranging from 9.6 to 12.5%.

Compared to the NAC method, the condyle-over-clivus ratio obtained using ACSC and ACSCRM methods shows a weak linear correlation (Fig. 5) with $R^2 = 0.67$ for the ACSC method, $R^2 = 0.51$ for the ACSCRM method and $R^2 = 0.56$ for the ACSCRM to ACSC method. There is a clear bias towards a higher ratio for the NAC method, with a mean difference of 5.5% for the ACSC method and 7.9% for the ACSCRM method.

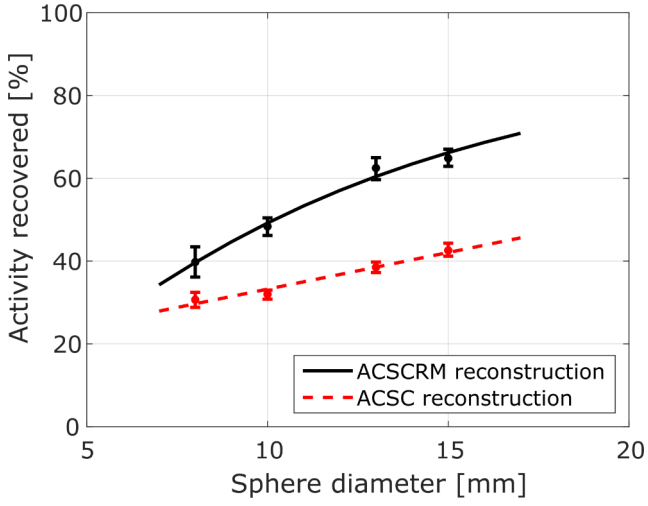

Fig. 3 The recovery curves obtained by measuring the asymmetric anthropomorphic phantoms. The recovery curve for the fully corrected (AC SC RM) reconstructions is fit using the two-parameter logistics function from the NEMA recovery curves (a = 553, b = 0.58). The recovery curve for the reconstructions without RM is best fit using a linear model (y = 0.018x + 0.16). All clinically relevant values are within the range of the experimental values

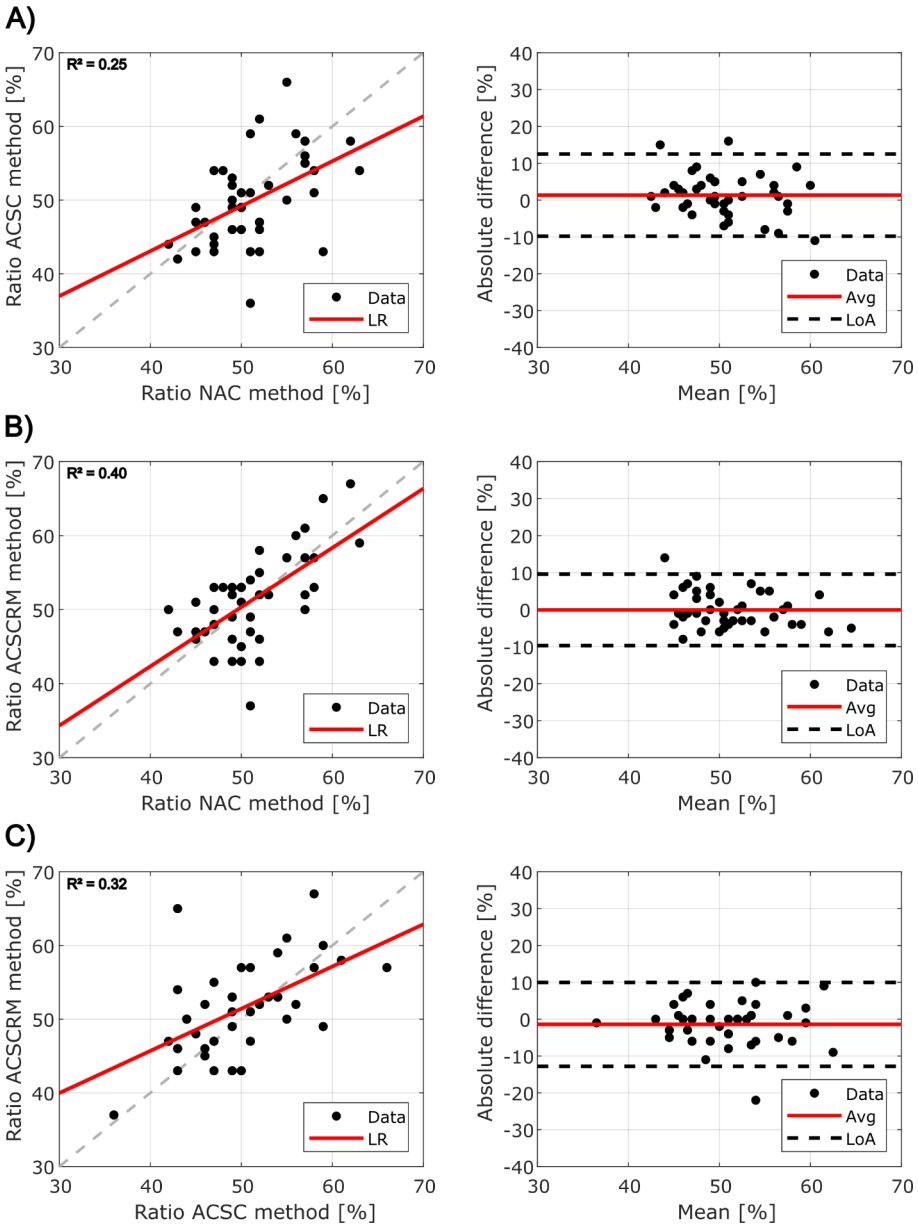

Fig. 4 The Bland-Altman plots for (**A**) the ACSC method compared to the reference method, (**B**) the ACSCRM method compared to the reference method, and (**C**) the ACSC method compared to the ACSCRM method

This was expected as attenuation correction will have a larger impact on the deeper lying clivus.

When applying the 55%:45% threshold to the quantitative reconstruction subset of the scans negative for asymmetric or bilateral growth (Supplementary Table 2), 2/13 (15%; 95% CI 0–35%) scans previously scored negative using the NAC method were reclassified as positive, and 13/19 (68%; 95% CI 48–89%) positive scans were reclassified as negative in the ACSC set (p=0.004). For the ACSCRM sets, 2/13 (15%; 95% CI 0–35%) scans that are reclassified as positive and 10/19 (53%; 95% CI 30–75%) would be reclassified as negative (p=0.038). Similarly, the subset of the scans positive for asymmetric or bilateral growth are classified according to the same 55%:45% threshold. 4/9 (44%; 95% CI 12–76%) scans previously scored positive using the NAC method were reclassified

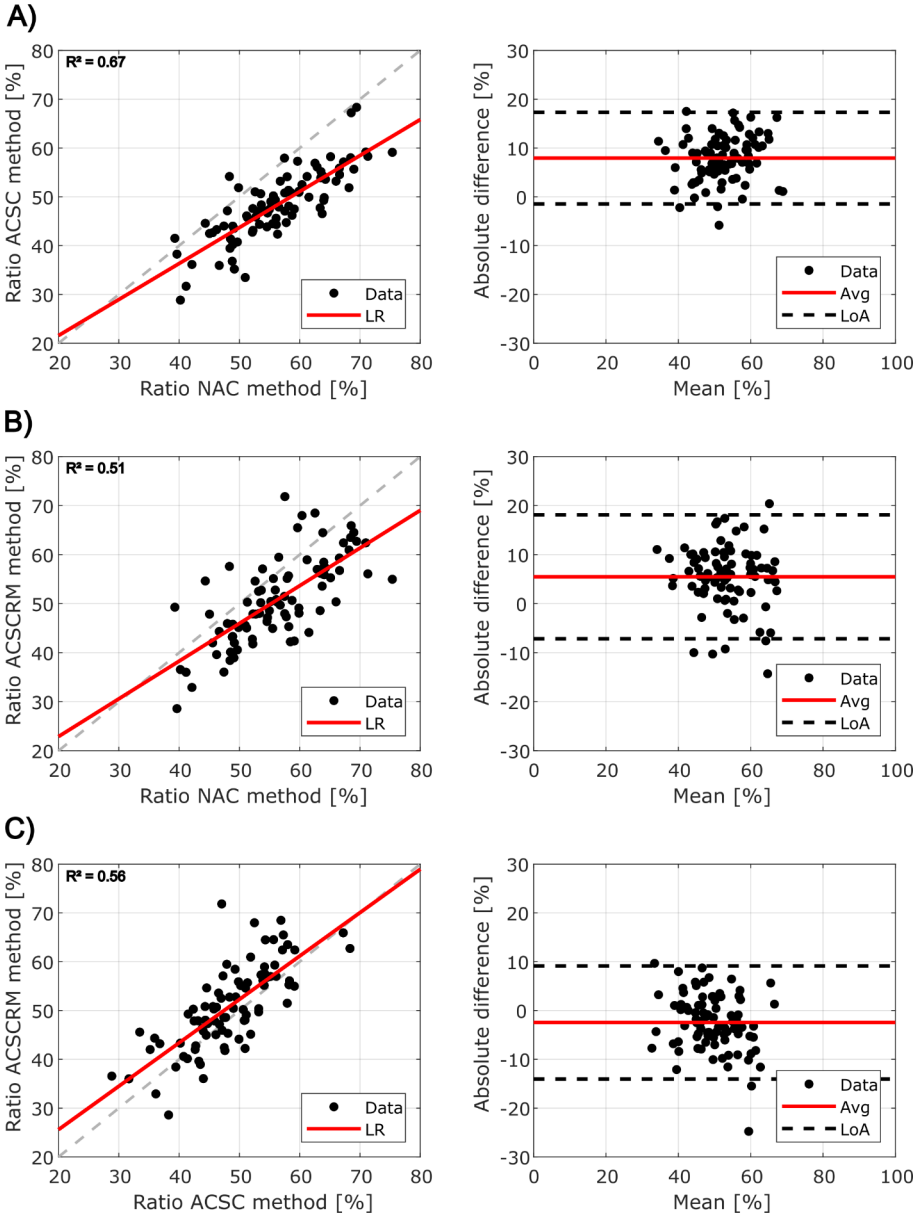

Fig. 5 The Bland-Altman plots of the condyle-over-clivus ratio for (**A**) the ACSC method compared to the reference method, (**B**) the ACSCRM method compared to the reference method, and (**C**) the ACSC method compared to the ACSCRM method

as negative, and 0/2 (0%; 97.5% CI 0–84%) negative scans were reclassified as positive in the ACSC set ($p=0.250$). For the ACSCRM sets, 0/9 (0%; 97.5% CI 0–34%) scans that are reclassified as positive and 1/2 (50%; 95% CI 0–100%) would be reclassified as negative ($p=1.000$). The results did not improve when using the suggested thresholds from Karssemakers et al. [10] of 12% and 8% (data not shown). Finally, the tracer uptake in the condyles was corrected using the partial volume correction factors derived from the anthropomorphic phantoms (Supplementary Table 3). However, correcting the ACSC and ACSCRM datasets using PVC did not result in significant changes in the reclassification in the UCH positive or negative cohorts (all $p>0.25$).

Overall, ACSCRM provided the highest combined sensitivity (91%; 95% CI 59–100%) and specificity (66%; 95% CI 47–81%) of all methods, while both ACSC and ACSCRM considerably improved specificity compared to the NAC method. No statistically significant improvements in sensitivity were seen between the different methods in this limited dataset (Fig. 6).

Discussion

Several reference structures have been proposed to compare bone tracer uptake in the mandibular condyles, including L4 [32] and C3 vertebrae and the clivus [5]. While the clivus is conveniently within the SPECT/CT field of view of the mandibular condyles, the limited diagnostic accuracy casts doubt it is an appropriate reference. This could be due to the differences in the physiology of bone remodeling, histology, pharmacokinetics, or other factors. For example, there is a difference in bone remodeling resulting from repeated stress on the mandible through the forces of mastication. Nevertheless, the clivus is the current clinically accepted reference structure [4, 8]. The assessment of bone tracer uptake in the mandibular condyles has traditionally been performed using planar or SPECT-only acquisitions. While SPECT/CT has replaced SPECT as the preferred modality for bone imaging [3], a prospective evaluation of the diagnostic accuracy of this modality was only recently performed and used the same semiquantitative approach described almost 40 years ago [10]. So far, studies have neglected the impact of incremental technological advances on image assessment, including reconstruction methods and the availability of absolute quantification. Yet, the mandibular condyles provide several challenges that can test the limits of commonly used correction techniques, including attenuation and scatter correction, and resolution modeling, justifying an in-depth analysis.

In the current study, anthropomorphic phantoms were developed and printed at a reasonable cost (purchase: 6k€) to mimic the complex anatomy of the skull base and the mandibular condyles, and serve as ground truth to validate bone SPECT/CT quantification in the evaluation of UCH. All prints were of sufficient quality, and excellent

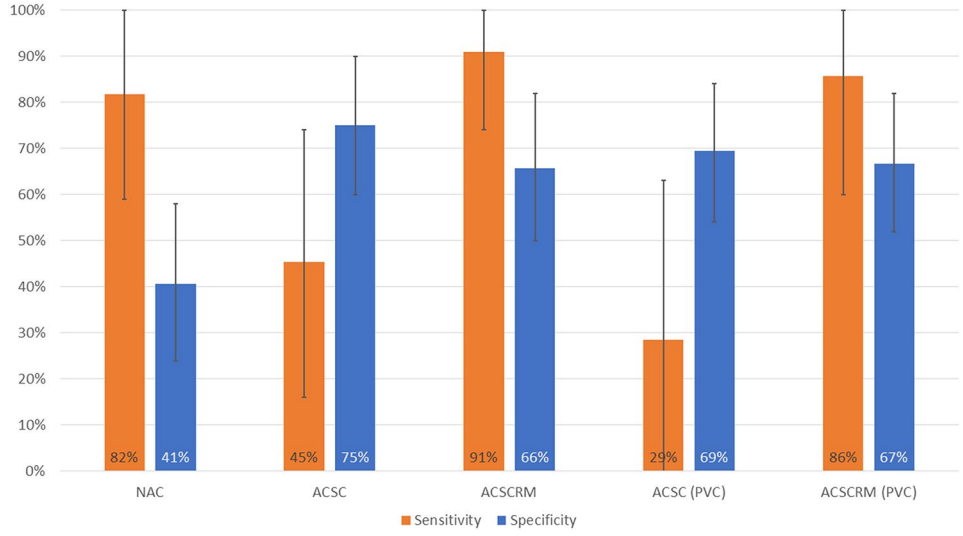

Fig. 6 The sensitivity and specificity of the classification according to the 55%:45% threshold for each reconstruction method

agreement with the volume segmented on the corresponding bone CT was observed, thereby providing unprecedented access to ground truth measurements. K_2HPO_4 as a high-density fluid to reproduce bone-like attenuation properties, has previously been used in a model of vertebral bone metastases and impacts activity recovery. Nevertheless, a direct comparison of the results with the current study is limited due to the higher target-to-background ratios in malignant disease, the use of larger size spheres (13 –28 mm compared to 8 –15 mm), and the routine use of RM by these authors.

For all sizes, only partial recovery was observed. As the same stock solution was used for the background regions of the symmetric and asymmetric phantoms, the smaller size of the symmetric phantom is the most probable reason for the lack of full recovery (range 63.1–82.2%). The recovery of the clivus as a function of its size was beyond the scope of this study. Still, it could significantly impact the use of the clivus as a reference region. This lack of full recovery, even for larger geometries, confirms the importance of anthropomorphic phantoms, as demonstrated, for example, in 2-compartment models of the kidney [33].

Considering the value of uptake ratios, the 95% confidence interval of the ACSC reconstruction included values beyond the 55%:45% threshold, potentially leading to a false classification for active growth. This overlap suggests a preference for the inclusion of RM in the reconstruction.

While there is already a long history of PVC in emission tomography, there is no definitive solution on handling small volumes in SPECT/CT [25]. The results from the NEMA IEC body phantom confirm the importance of spatial orientation with the scan field, with a significantly different recovery curve for different positions [13]. This is at least partially due to the dependence of the spatial resolution on the distance between the detector and the object of interest, as confirmed in a recent study using Monte Carlo simulation [34]. Given the lack of a general solution to this problem and the earlier results demonstrating the influence of local anatomy, a methodology for PVC was proposed using the developed pathology-specific anthropomorphic phantoms. This allows for an integration of the correct spatial relationships between the different regions of interest with the correct geometry and attenuating properties. Absolute quantification was considerably improved when applying the recovery coefficients from the asymmetric anthropomorphic phantom to the symmetric anthropomorphic phantom, with the activity recovery increasing to above 74%. Importantly, the improvement was consistent for the ACSC and ACSCRM sets and their respective RCs. This highlights the relevance of anthropomorphic phantoms over the generally considered NEMA phantom for partial volume correction in SPECT/CT.

In the retrospective analysis, the correlation and agreement for the ACSC and ACSCRM methods with the current clinical standard is limited. The largest impact was observed on the activity recovery for the clivus with the use of attenuation correction which can be explained by the position of the clivus deeper in the skull. Overall, it is clear from the comparison of the different techniques that the attenuation and scatter correction (due to the high density of bone) and resolution modeling (due to the size of the condyles) significantly affect the classification of UCH using the historically established thresholds. The significant differences in the clinically considered disease-negative population suggest an improvement in specificity when using the quantitative reconstructions while simultaneously considering asymmetric and bilateral growth thresholds. The

retrospective analysis of the clinical data shows that, as the physics of the NAC method and ACSC(RM) method(s) are very different, the improvement in quantitative accuracy due to the attenuation correction could provide an important contribution to the diagnostic accuracy. These findings underscore the importance of validating existing image analysis techniques and thresholds whenever novel technology is introduced in clinical practice [35].

Although this study was performed on a single SPECT/CT system, the results reported by Peters et al. demonstrated that vendor-neutral reconstructions allow for reproducible results when comparing NEMA phantom scans across Anger-type systems of different vendors [36]. For this reason, rather than using the vendor-specific reconstruction and analysis platform, a vendor-neutral alternative was used. Currently, these results have not been confirmed when including novel ring-geometry systems for ^{99m}Tc. However, combined results from Peters et al. [37] and Nuttens et al. [38] suggest this should be feasible for ^{177}Lu.

In summary, we have shown that application-specific anthropomorphic phantoms are superior to generic phantoms to determine the optimal correction methods for bone SPECT/CT. In addition, significant improvements in specificity were seen with ACSC and ACSCRM methods, while ACSCRM provided the best diagnostic test characteristics in an initial retrospective analysis. These results suggest that absolute quantification may provide independent information beyond the semiquantitative assessment in current routine clinical use. Nevertheless, further standardization and harmonization of image acquisition, reconstruction and analysis is required when defining thresholds that should be universally reproducible in clinical datasets.

Limitations

A limitation of the current phantom study is that it could not be established whether the approximation of the condyles as ellipsoids was valid. The retrospective study includes a small number of patients (N=27). Given the small number of positive cases, any analysis of the diagnostic sensitivity was limited.

Conclusions

Anthropomorphic phantoms were shown to be essential in determining optimal settings for acquisition, reconstruction, and analysis. A significant improvement in partial volume correction was achieved by using appropriate anthropomorphic phantoms rather than the NEMA phantom, which should be avoided when possible. Clinically relevant reclassification rates for the diagnosis of UCH were observed between various methods, suggesting an improvement in specificity for the quantitative reconstruction sets.

Abbreviations

AC	Attenuation correction
CT	Computed tomography
OSEM	Ordered-subsets expectation maximization
PVC	Partial volume correction
PVE	Partial volume effect
RC	Recovery coefficient
RM	Resolution modeling
ROI	Region-of-interest
SC	Scatter correction
SPECT	Single-photon emission computed tomography
UCH	Unilateral condylar hyperplasia
VOI	Volume-of-interest

Supplementary Information

The online version contains supplementary material available at https://doi.org/10.1186/s40658-024-00676-6.

Supplementary Material 1

Author contributions

SDS planned the study, developed and produced the phantoms, acquired image data, performed the analysis and wrote the manuscript. TVdW planned the study, analyzed the data and wrote the manuscript. JCD planned the study and critically revised the manuscript. GG, EVdC and WDV critically revised the manuscript. All authors read and approved the final manuscript.

Funding

Not applicable.

Data availability

Data are available upon request to the corresponding author.

Declarations

Ethics approval and consent to participate

This study was approved by the ethics committee of the Antwerp University Hospital (N°: 5640).

Consent for publication

Not applicable.

Competing interests

The authors declare that they have no competing interests.

Received: 26 March 2024 / Accepted: 5 August 2024

Published online: 23 August 2024

References

1. Higginson JA, Bartram AC, Banks RJ, Keith DJW. Condylar hyperplasia: current thinking. Br J Oral Maxillofac Surg. 2018;56(8):655–62.
2. ElNaghy R, Hasanin M. Impact of malocclusions on oral health-related quality of life among adolescents. Evid Based Dent. 2023;24(3):140–1.
3. Van den Wyngaert T, Strobel K, Kampen WU, Kuwert T, van der Bruggen W, Mohan HK, et al. The EANM practice guidelines for bone scintigraphy. Eur J Nucl Med Mol Imaging. 2016;43(9):1723–38.
4. Saridin CP, Raijmakers PG, Tuinzing DB, Becking AG. Bone scintigraphy as a diagnostic method in unilateral hyperactivity of the mandibular condyles: a review and meta-analysis of the literature. Int J Oral Maxillofac Surg. 2011;40(1):11–7.
5. Saridin CP, Raijmakers PG, Al Shamma S, Tuinzing DB, Becking AG. Comparison of different analytical methods used for analyzing SPECT scans of patients with unilateral condylar hyperactivity. Int J Oral Maxillofac Surg. 2009;38(9):942–6.
6. Israel O, Pellet O, Biassoni L, De Palma D, Estrada-Lobato E, Gnanasegaran G, et al. Two decades of SPECT/CT - the coming of age of a technology: an updated review of literature evidence. Eur J Nucl Med Mol Imaging. 2019;46(10):1990–2012.
7. Van den Wyngaert T, Palli SR, Imhoff RJ, Hirschmann MT. Cost-effectiveness of bone SPECT/CT in painful total knee arthroplasty. J Nucl Med. 2018;59(11):1742–50.
8. Chan BH, Leung YY. SPECT bone scintigraphy for the assessment of condylar growth activity in mandibular asymmetry: is it accurate? Int J Oral Maxillofac Surg. 2018;47(4):470–9.
9. Rushinek H, Tabib R, Fleissig Y, Klein M, Tshori S. Evaluation of three analysis methods for (99m)tc MDP SPECT scintigraphy in the diagnosis of unilateral condylar hyperplasia. Int J Oral Maxillofac Surg. 2016;45(12):1607–13.
10. Karssemakers LHE, Nolte JW, Rehmann C, Raijmakers PG, Becking AG. Diagnostic performance of SPECT-CT imaging in unilateral condylar hyperplasia. Int J Oral Maxillofac Surg. 2023;52(2):199–204.
11. Dewaraja YK, Frey EC, Sgouros G, Brill AB, Roberson P, Zanzonico PB, et al. MIRD pamphlet 23: quantitative SPECT for patient-specific 3-dimensional dosimetry in internal radionuclide therapy. J Nucl Med. 2012;53(8):1310–25.
12. De Schepper S, Ritt P, Van den Wyngaert T, Kuwert T. Quantitative radionuclide imaging of bone metastases. Q J Nucl Med Mol Imaging. 2019;63(2):129–35.
13. Dickson JC, Armstrong IS, Gabina PM, Denis-Bacelar AM, Krizsan AK, Gear JM, et al. EANM practice guideline for quantitative SPECT-CT. Eur J Nucl Med Mol Imaging. 2023;50(4):980–95.
14. Chun SY, Fessler JA, Dewaraja YK. Correction for collimator-detector response in SPECT using point spread function template. IEEE Trans Med Imaging. 2013;32(2):295–305.
15. Chiesa C, Sjogreen-Gleisner K, Walrand S, Strigari L, Flux G, Gear J, et al. EANM dosimetry committee series on standard operational procedures: a unified methodology for (99m)Tc-MAA pre- and (90)Y peri-therapy dosimetry in liver radioembolization with (90)Y microspheres. EJNMMI Phys. 2021;8(1):77.
16. Sjogreen Gleisner K, Chouin N, Gabina PM, Cicone F, Gnesin S, Stokke C, et al. EANM dosimetry committee recommendations for dosimetry of 177Lu-labelled somatostatin-receptor- and PSMA-targeting ligands. Eur J Nucl Med Mol Imaging. 2022;49(6):1778–809.
17. De Schepper S, Gnanasegaran G, Dickson JC, Van den Wyngaert T. Absolute quantification in diagnostic SPECT/CT: the Phantom Premise. Diagnostics (Basel). 2021;11(12).
18. Gear JI, Cummings C, Craig AJ, Divoli A, Long CD, Tapner M, et al. Abdo-Man: a 3D-printed anthropomorphic phantom for validating quantitative SIRT. EJNMMI Phys. 2016;3(1):17.

19. Tran-Gia J, Schlogl S, Lassmann M. Design and fabrication of kidney phantoms for Internal Radiation Dosimetry using 3D Printing Technology. J Nucl Med. 2016;57(12):1998–2005.
20. Tran-Gia J, Lassmann M. Optimizing image quantification for (177)Lu SPECT/CT based on a 3D printed 2-Compartment kidney Phantom. J Nucl Med. 2018;59(4):616–24.
21. Fukami M, Matsutomo N, Yamamoto T. Optimization of number of iterations as a Reconstruction parameter in bone SPECT imaging using a novel thoracic spine Phantom. J Nucl Med Technol. 2021;49(2):143–9.
22. Carass A, Roy S, Gherman A, Reinhold JC, Jesson A, Arbel T, et al. Evaluating White Matter Lesion segmentations with Refined Sorensen-Dice analysis. Sci Rep. 2020;10(1):8242.
23. Dreuille Od, Strijckmans V, Ameida P, Loc'h C, Bendriem B. Bone equivalent liquid solution to assess accuracy of transmission measurements in SPECT and PET. IEEE Trans Nucl Sci. 1997;44(3):1186–90.
24. Bland M. Chapter 20 clinical measurement. An introduction to Medical statistics. Fourth Edition ed: Oxford University Press; 2015.
25. Erlandsson K, Buvat I, Pretorius PH, Thomas BA, Hutton BF. A review of partial volume correction techniques for emission tomography and their applications in neurology, cardiology and oncology. Phys Med Biol. 2012;57(21):R119–59.
26. Thomas BA, Cuplov V, Bousse A, Mendes A, Thielemans K, Hutton BF, et al. PETPVC: a toolbox for performing partial volume correction techniques in positron emission tomography. Phys Med Biol. 2016;61(22):7975–93.
27. Gear JI, Cox MG, Gustafsson J, Gleisner KS, Murray I, Glatting G, et al. EANM practical guidance on uncertainty analysis for molecular radiotherapy absorbed dose calculations. Eur J Nucl Med Mol Imaging. 2018;45(13):2456–74.
28. Lopez DF, Rios Borras V, Munoz JM, Cardenas-Perilla R, Almeida LE. SPECT/CT correlation in the diagnosis of unilateral Condilar Hyperplasia. Diagnostics (Basel). 2021;11(3).
29. Bland M. Chapter 13 the analysis of cross-tabulations. An introduction to Medical statistics. Fourth Edition ed: Oxford University Press; 2015.
30. Dice LR. Measures of the Amount of Ecologic Association between Species. Ecology. 1945;26(3):297–302.
31. Kim T-H, Lee D-Y, Jung S-K. Comparison of Trabecular Bone Mineral Density Measurement Using Hounsfield Unit and Trabecular microstructure in Orthodontic patients using Cone-Beam Computed Tomography. Appl Sci. 2021;11(3):1028.
32. Kaban LB, Cisneros GJ, Heyman S, Treves S. Assessment of mandibular growth by skeletal scintigraphy. J Oral Maxillofac Surg. 1982;40(1):18–22.
33. Tran-Gia J, Denis-Bacelar AM, Ferreira KM, Robinson AP, Calvert N, Fenwick AJ, et al. A multicentre and multi-national evaluation of the accuracy of quantitative Lu-177 SPECT/CT imaging performed within the MRTDosimetry project. EJNMMI Phys. 2021;8(1):55.
34. Leube J, Gustafsson J, Lassmann MSR, Tran-Gia M. The art of Juggling: on the infuence of Sphere Positioning on Recovery coefcients determined using an IEC-NEMA Phantom. Eur J Nucl Med Mol Imaging. 2023;50(Suppl 1):S681.
35. Van den Wyngaert T, Elvas F, De Schepper S, Kennedy JA, Israel O. SPECT/CT: standing on the Shoulders of Giants, it is time to Reach for the Sky! J Nucl Med. 2020;61(9):1284–91.
36. Peters SMB, van der Werf NR, Segbers M, van Velden FHP, Wierts R, Blokland K, et al. Towards standardization of absolute SPECT/CT quantification: a multi-center and multi-vendor phantom study. EJNMMI Phys. 2019;6(1):29.
37. Peters SMB, Meyer Viol SL, van der Werf NR, de Jong N, van Velden FHP, Meeuwis A, et al. Variability in lutetium-177 SPECT quantification between different state-of-the-art SPECT/CT systems. EJNMMI Phys. 2020;7(1):9.
38. Nuttens V, Schramm G, D'Asseler Y, Koole M. Comparison of a 3D CZT and conventional SPECT/CT system for quantitative Lu-177 SPECT imaging. EJNMMI Phys. 2024;11(1):29.

Publisher's Note